Materials Chemistry and Physics 240 (2020) 122183

Contents lists available at ScienceDirect

Materials Chemistry and Physics

journal homepage: www.elsevier.com/locate/matchemphys

Thermomechanical, surface and shape memory properties of thermosetting blends of epoxy with Poly(ethylene oxide): An impact of POSS microdomain formation

Yanhao Zhang [a,b], Lei Li [a,*], Kangming Nie [b], Sixun Zheng [a,**]

[a] School of Chemistry and Chemical Engineering, Shanghai Jiao Tong University, Shanghai, 200240, PR China
[b] College of Chemistry and Chemical Engineering, Anhui University, Hefei, 230601, PR China

HIGHLIGHTS

- Effect of POSS on properties of epoxy/PEO-POSS nanocomposites was investigated.
- Epoxy/PEO-POSS nanocomposites displayed high thermal and mechanical properties.
- Formation of POSS microdomains accelerated shape recovery of nanocomposites.

GRAPHICAL ABSTRACT

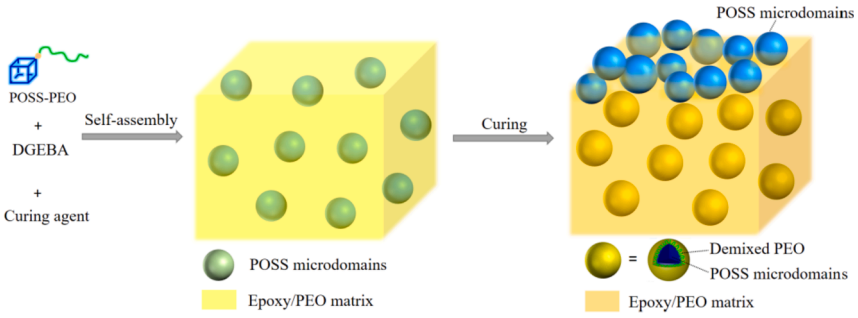

ARTICLE INFO

Keywords:
POSS
Epoxy
Nanocomposites
Microdomains
Shape memory properties

ABSTRACT

POSS is a class of unique building blocks for preparation of organic-inorganic nanocomposites. In this work, we investigated the influence of POSS microdomains on the properties of homogenous thermosetting blends of epoxy with poly(ethylene oxide). Herein, we first synthesized POSS-terminated poly (ethylene oxide) (PEO-POSS) and then incorporated it into epoxy to afford epoxy/PEO-POSS nanocomposites. Incorporation of PEO-POSS resulted in a microphase separation in the materials due to the self-assembly of PEO-POSS in the epoxy matrix. The influence of POSS microdomains on thermomechanical, surface and shape memory properties of nanocomposites were investigated in detail. Epoxy/PEO-POSS nanocomposites displayed higher glass transition temperature and surface hydrophobicity than epoxy/PEO blends with the same PEO content. Moreover, the formation of POSS microdomains could accelerate the shape recovery rate of the materials.

1. Introduction

Epoxies are a class of important thermosetting polymers. They have been widely used as adhesive, coating and structural materials due to the excellent mechanical properties, chemical resistance and ease of processing et al. [1–4]. However, due to the inherent limitations (*e.g.* low toughness), it is necessary to modify the epoxy resin to satisfy the requirements as functional materials [5–8]. Under this circumstance,

* Corresponding author.
** Corresponding author.
E-mail addresses: lli_sjtu@163.com (L. Li), szheng@sjtu.edu.cn (S. Zheng).

https://doi.org/10.1016/j.matchemphys.2019.122183
Received 4 July 2019; Received in revised form 12 September 2019; Accepted 14 September 2019
Available online 17 September 2019

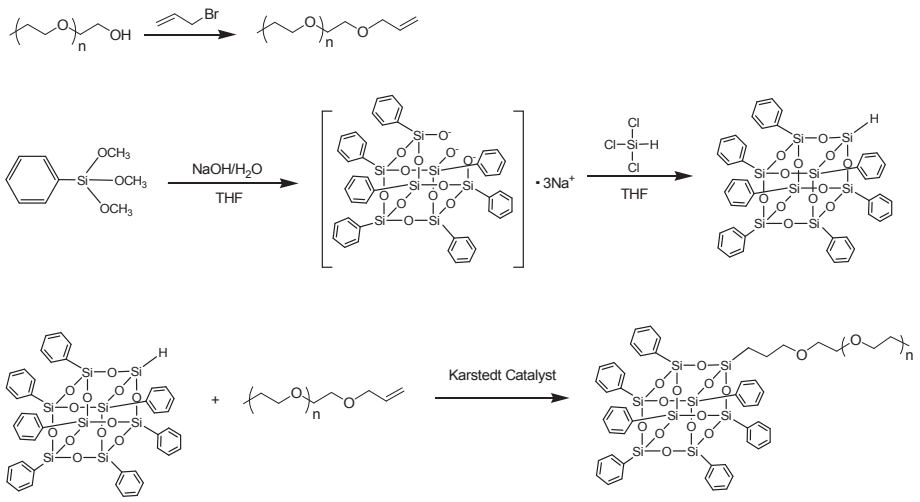

Scheme 1. Synthesis of PEO-POSS.

epoxy based composites have been attracted much attention. Depending on the different applications, epoxy resins have been functionalized by compounding with organic polymers or inorganic components [9–20]. Among them, introducing inorganic components in epoxy resin is an important method to achieve enhanced performance with the synergistic effect of organic and inorganic components.

Polyhedral oligomeric silsesquioxane (POSS) is a class of organic-inorganic nanobuilding blocks. It has received considerable attention as the modifiers of the organic polymers due to its unique structure, which is composed of nanosized inorganic framework and organic ligands covalently bonded to Si atoms [21,22]. Incorporation of POSS macromers into epoxy thermosets is able to improve their thermal, oxidative, and dimensional stability, *etc* [23–29]. It is realized that the composites with nanosized mixing can optimize the inter-component interactions in the thermosets, affording an efficient way to solve the problems associated with the interface. In the last decades, many nanocomposites have been designed by using functionalized POSS derivatives in conjunction with epoxy thermosets. In contrast with the plain epoxy and macrophase-separated epoxy composites, epoxy/POSS nanocomposites displayed excellent properties such as the high thermal stability, high surface hydrophobicity, high mechanical properties and low dielectric constant, *etc* [30–33]. Generally, epoxy/POSS nanocomposites can be prepared *via* chemical and physical approach. The chemical approach is related to that POSS macromers bearing reactive groups such as amine groups, epoxide groups, hydroxyl groups can be reacted with epoxy precursors (*i.e.* DGEBA) during curing process [24,34–40]. POSS can be well dispersed in the epoxy matrix at a molecular segmental or nanosized level. For instance, Laine et al. [36] synthesized multifunctional POSS macromer: octakis (glycidyldimethylsiloxy) octasilsesquioxane and incorporated it into epoxy to obtain the nanocomposites. It is found that POSS was dispersed into epoxy thermosets at a molecular level. The existence of POSS and the well dispersion improved the thermal stability, tensile moduli and fracture toughness of the materials. The other approach to get epoxy/POSS nanocomposites is physical blending [41–44]. In contrast with the direct blending of POSS macromers with epoxy, herein, physical blending approach for the preparation of epoxy/POSS nanocomposites is based on self-assembly mechanism. The prerequisite of this approach is to synthesize a POSS-containing amphiphilic polymer, in which POSS is immiscible with epoxy while the other block is miscible with epoxy after curing process. In this case, the amphiphilic polymer will assemble into nano-objects in the epoxy matrix. For example, Zheng et al. [42,43] synthesized a POSS-terminated poly (ε-caprolactone) (POSS-PCL) and cured it with DEGBA in the presence of 4,4′-methylene-bis(2-chloroaniline). In the composites, POSS aggregated into microdomains with the size of 20–30 nm due to POSS-POSS interaction. The nanocomposites displayed high thermal stability and surface hydrophobicity. Notably, the properties of these nanocomposites are attributed to a combination of POSS and the polymer/epoxy matrix. As a consequence, the influence of POSS microdomains on the properties of the miscible/homogenous thermosetting blends is worth studying.

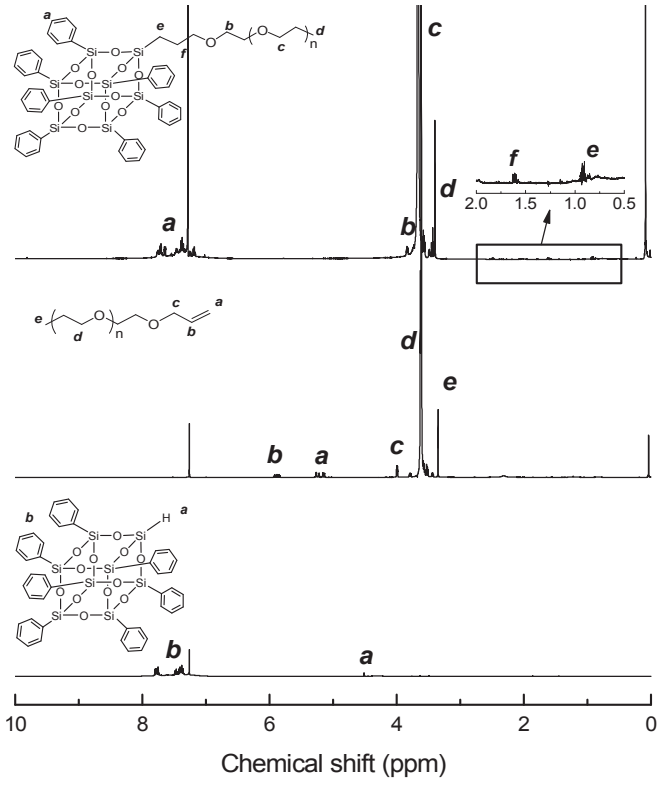

Fig. 1. ^{1}H NMR spectra of H-POSS, vinyl-PEO and PEO-POSS.

In this work, we prepared POSS-containing nanocomposites and further explored the influence of POSS on the properties of miscible/homogenous thermosetting blends. Towards this end, we synthesized POSS-terminated poly (ethylene oxide) (PEO-POSS) and blended it with epoxy resins to afford epoxy/PEO-POSS nanocomposites. Since PEO is miscible with epoxy and POSS is immiscible with epoxy [45,46], it is expected that PEO-POSS will display self-assembly behavior in the epoxy resin. The morphologies of epoxy/PEO-POSS nanocomposites

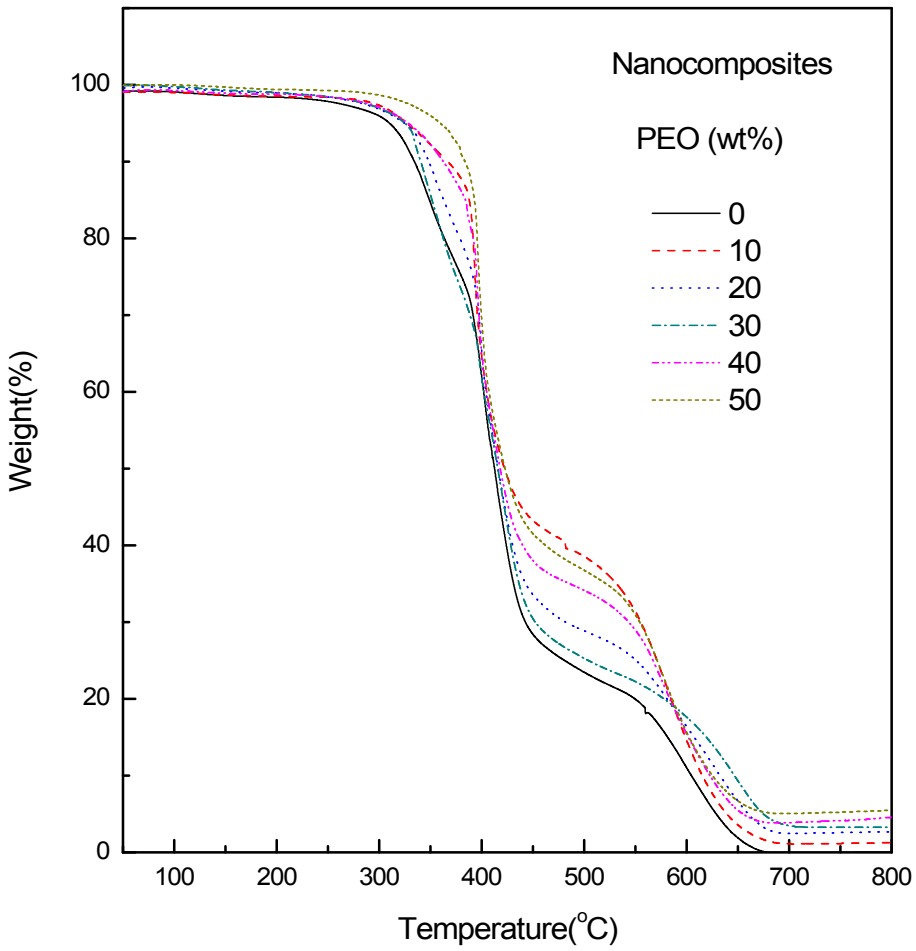

Fig. 2. TGA curves of the epoxy/PEO-POSS nanocomposites.

Table 1
The composition of PEO-POSS/epoxy nanocomposites.

Nanocomposites PEO (wt%)	T_d[a]	Residues	POSS content (wt%)[b]	POSS content (wt%)[c]
0	315.2	0	0	0
10	330.1	1.31	2.61	1.96
20	329.6	2.49	4.96	3.92
30	328.5	3.23	6.43	5.66
40	332.5	4.27	8.50	7.41
50	364.2	5.23	10.41	9.09

[a] The degradation temperature at 5 wt% of weight loss.
[b] POSS content calculated according to the residues of TGA results.
[c] POSS content calculated according to the mass feed ratio.

were investigated by transmission electron microscope (TEM). In comparison, we also prepared epoxy/PEO blends with the same content of PEO as epoxy/PEO-POSS. The effect of POSS on the thermal and surface properties of materials were investigated by dynamic mechanical thermal analysis (DMTA), thermogravimetric analysis (TGA), atom force microscope (AFM) and contact angle measurements. In addition, the formation of POSS microdomains is expected to endow the nanocomposites with low and tunable shape memory transition temperature as well as the accelerated recovery rate. The shape memory properties of epoxy/PEO-POSS nanocomposites were also investigated in detail.

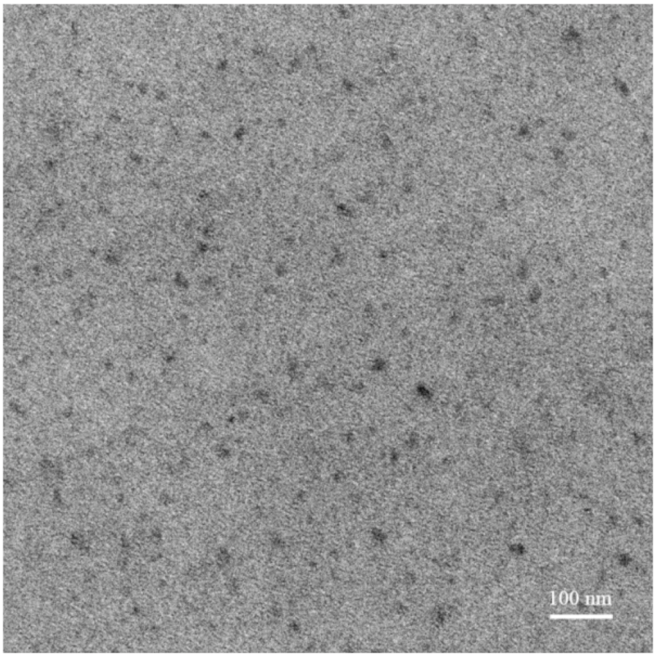

Fig. 3. TEM image of epoxy/PEO-POSS nanocomposite with PEO content of 20 wt%.

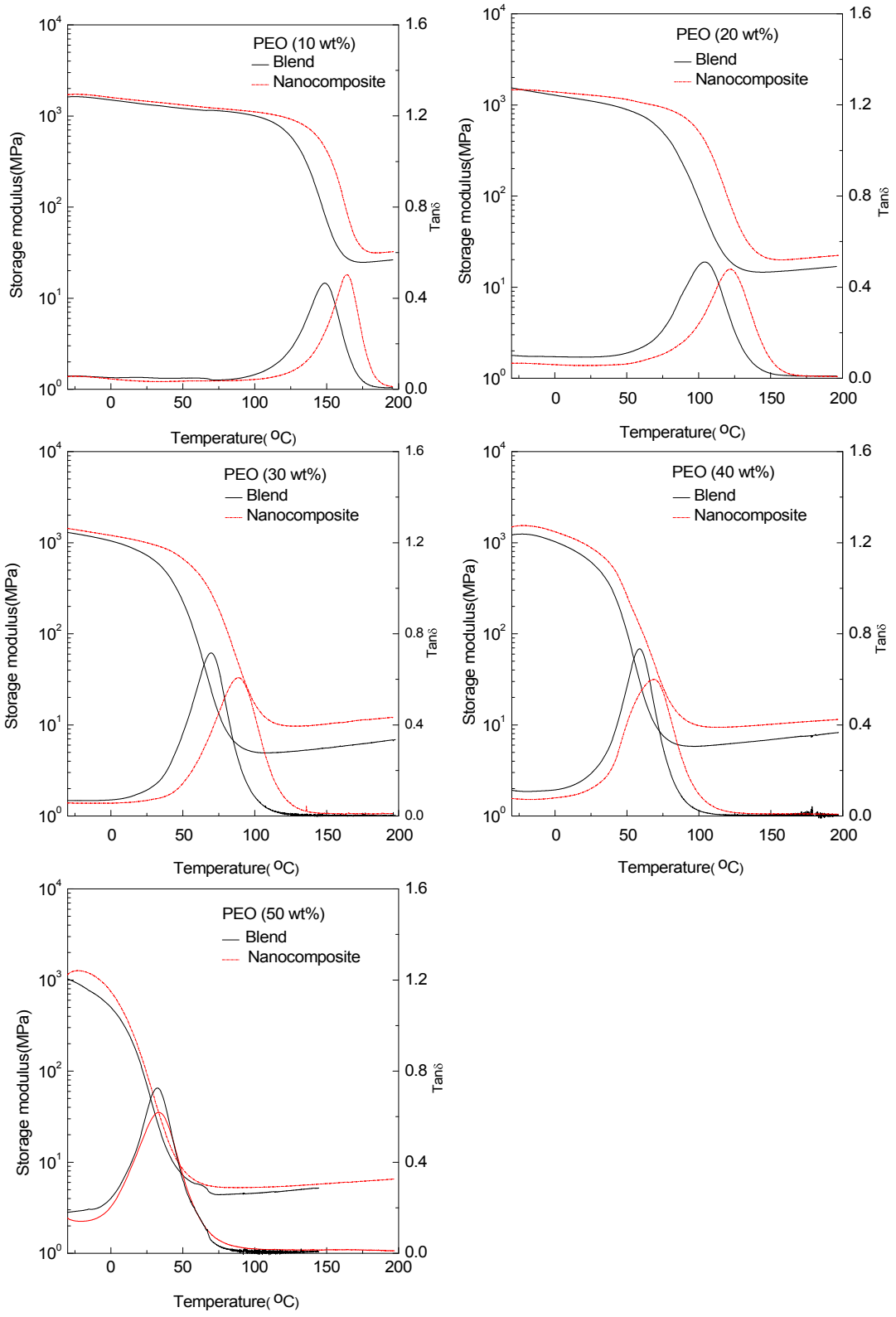

Fig. 4. DMTA curves of epoxy/PEO blends and epoxy/PEO-POSS nanocomposites.

2. Experimental

2.1. Materials

Phenyltrimethoxysilane was purchased from Jining Chemical Technology Co., China. Before use, it was purified by distilling under reduced pressure. Allyl bromide, sodium hydride, trichlorosilane and poly (ethylene oxide) monomethyl ether with the molecular weight of 5,000 were purchased from Alfa Aesar Co., China. Diglycidyl ether of bisphenol A epoxy monomer (E51) and the curing agent (DDM) were available from Shanghai resin Co., China and Alfa Aesar Co., China, respectively. Sodium hydroxide, tetrahydrofuran, dichloromethane,

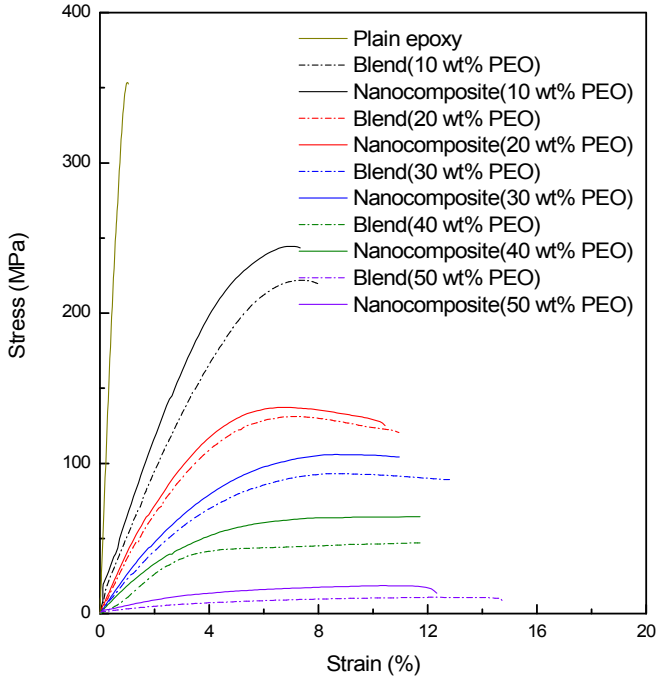

Fig. 5. Strain-stress curves of epoxy/PEO blends and epoxy/PEO-POSS nanocomposites.

methanol and diethyl ether were purchased from Shanghai Chemical Reagent Co. China.

2.2. Synthesis of POSS-terminated PEO

POSS-terminated PEO was synthesized *via* a hydrosilation reaction between an allylic-terminated PEO and hydroheptaphenyl POSS (H-POSS) in the presence of Karstedt catalyst. Allylic-terminated PEO was synthesized by following the literature [41]. Typically, NaH (0.672 g, 14 mmol) and anhydrous THF (30 ml) were charged to a 250 ml flask, and then the THF solution of PEO (10.500 g, 2.1 mmol) was slowly dropped into the flask at 0 °C. The reaction was performed at room temperature for 3 h and then the THF solution of allylic bromide (1.660 g, 14 mmol) was dropwise added into the mixture. The reaction was performed at room temperature for 24 h. After reaction, the insoluble solids were filtered out. The filtrate was concentrated and dropped into a great amount of diethyl ether to obtain the precipitates. After drying, the product (9.58 g) was obtained with a yield of 91%. ^{1}H NMR (ppm, $CDCl_3$): 3.25 (*s*, -O-C***H***$_3$), 3.65 (*s*, C***H***$_2$–C***H***$_2$–O), 4.01 (*s*, CH_2═CHC***H***$_2$O-), 4.55 (*m*, CH_2═C***H***CH_2O-), 5.52 (*m*, C***H***$_2$═$CHCH_2$O-).

H-POSS were synthesized according to our previous research work [47]. The as-synthesized allylic-terminated PEO and H-POSS were then performed hydrosilation reaction to obtain PEO-POSS. Allylic-terminated PEO (5.000 g, 1 mmol) and H-POSS (1.100 g, 1.12 mmol) were dissolved in 100 mL of anhydrous toluene. The mixture was purged highly pure nitrogen for 30 min and 20 μL of Karstedt catalyst was injected into the mixture. Afterwards, the mixture was heated to 90 °C and the reaction was performed at 90 °C for 24 h. After reaction, toluene was removed by a rotary evaporator, and the remained solution was precipitated into 100 mL of diethyl ether. After drying, PEO-POSS was obtained with a yield of 70.2%. ^{1}H NMR ($CDCl_3$, ppm): 3.25 (*s*, -O-C***H***$_3$), 3.65 (*s*, C***H***$_2$–C***H***$_2$–O), 7.15–7.80 (*m*, protons of phenyl groups).

2.3. Preparation of thermosetting blends

Desired amount of PEO-POSS and DGEBA were weighed into a baker and melted in an oven at 100 °C. After the mixture is homogenous, DDM

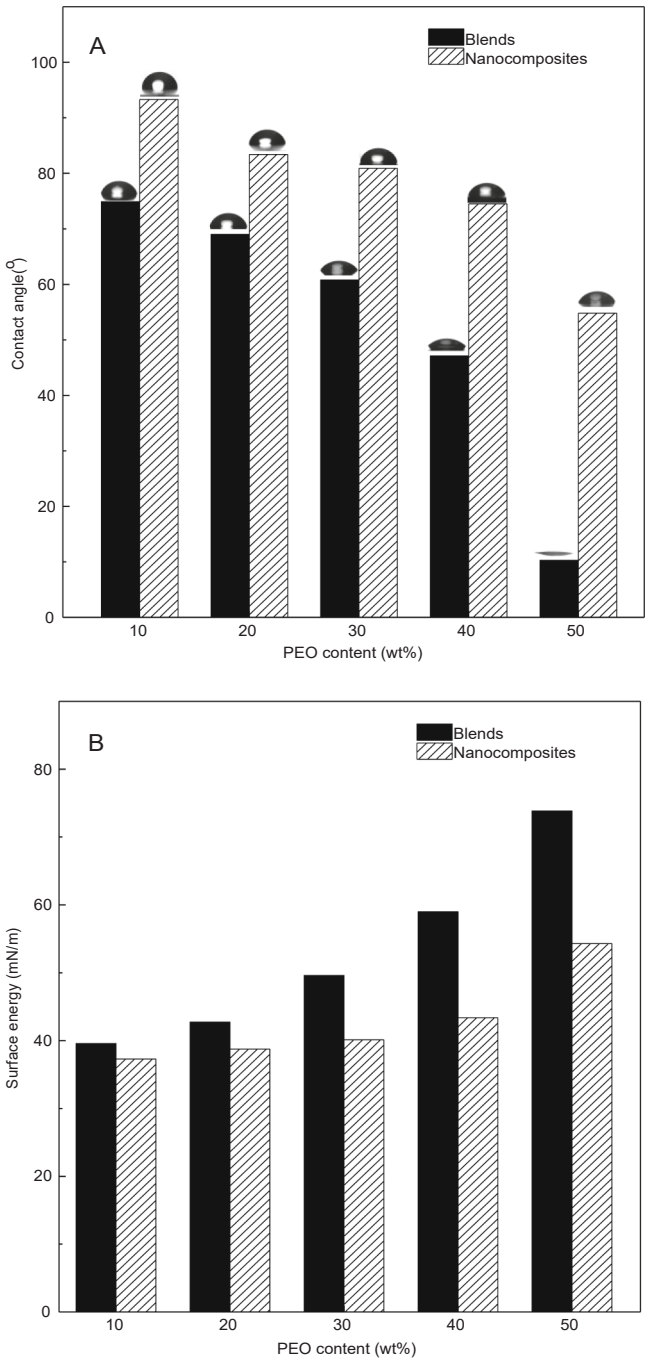

Fig. 6. Water contact angles up) and surface energy down) of epoxy/PEO blends and epoxy/PEO-POSS nanocomposites.

with equal mole content of amine to that of epoxide groups of DGEBA was introduced into the baker, which was then stirred vigorously to make the system transparent. Next, the mixture was poured into an aluminum pan. The samples were thermally cured at 150 °C for 3 h and at 180 °C for 2 h. In order to investigate the effect of POSS on the properties of epoxy thermosets, epoxy/PEO thermosets with the same content of PEO as epoxy/PEO-POSS thermosets were also prepared.

2.4. Measurements

^{1}H NMR measurements were carried out on a Varian Mercury Plus 400 MHz NMR spectrometer and deuterium chloroform was used as the

Table 2
Surface properties of epoxy/PEO blends and epoxy/PEO-POSS nanocomposites.

PEO (wt%)	Samples	Contact angle (°) H_2O	CH_2I_2	Surface energy (mN/m) γ_s^d	γ_s^p	γ_s
10	Blend	74.90	44.10	32.21	7.37	39.58
	Nanocomposite	93.30	44.90	36.55	0.72	37.27
20	Blend	69.00	41.00	32.54	10.20	42.74
	Nanocomposite	83.40	42.10	35.58	3.28	38.76
30	Blend	60.80	29.50	36.34	13.27	49.61
	Nanocomposite	80.90	39.80	36.25	3.87	40.12
40	Blend	47.10	12.50	38.81	20.20	59.00
	Nanocomposite	74.50	34.80	37.27	6.09	43.36
50	Blend	10.30	9.50	34.57	39.29	73.86
	Nanocomposite	54.80	20.30	38.40	15.85	54.30

solvent. The morphological observations of POSS-containing nanocomposites in bulk were performed on a JEOLJEM 2100F TEM at a voltage of 200 kV. The nanocomposites were cut into ultrathin films with the thickness of 100 nm. The films were observed without any treatment. The surface morphological observations of epoxy/PEO-POSS nanocomposites were performed on CSPM5500 atom force microscope with a tapping mode. The scanning rate was 2.0 Hz. The cured samples were scanned without any treatment. TA Q5000 thermal gravimetric analyzer was used to investigate the formation of organic-inorganic nanocomposites. The samples were heated from 50 °C to 800 °C under air atmosphere at a heating rate of 20 °C/min. The measurement of contact angle was carried out on a DSA30 instrument. Dynamic mechanical properties were measured by a DMTA Q800 instrument to obtain the storage modulus and loss tangent (tan δ) messages. The measurements were performed in a stretch mode at a frequency of 1 Hz and a heating rate of 3 °C/min. Tensile mechanical tests were performed on an electron testing instrument (Songdun Instrument Co. Ltd, China). The dog bone-shaped specimens were prepared for the measurements. The stretching rate was 10 mm/min. Consecutive shape memory cycles were also carried out on a DMTA Q800 instrument. The samples were first heated to T_1 (20 °C above T_g), and elongated at T_1 until the stress increased to 0.6 MPa at the rate of 0.06 MPa/min. With the elongated shape, the sample was cooled to a low temperature (T_2) at the rate of 3 °C/min to fix the sample. Afterwards, the stress was decreased to 0 MPa at the rate of 0.06 MPa/min at T_2. Finally, the sample was heated to T_1 at the rate of 3 °C/min to recover the shape. The measurements were repeated five times.

3. Results and discussion

3.1. Synthesis of POSS-terminated PEO

POSS-terminated PEO (PEO-POSS) was synthesized *via* a hydrosilation reaction between allylic-terminated PEO and hydroheptaphenyl POSS (H-POSS) in the presence of Karstedt catalyst (Scheme 1). The chemical structure of allylic-terminated PEO, H-POSS and PEO-POSS were confirmed by ^{1}H NMR spectra (Fig. 1). The resonance signal of protons for Si–H groups of H-POSS and allylic groups of allylic-terminated PEO were detected at 4.51, 4.55, 5.52 ppm, respectively. After hydrosilation, the above resonance signals disappeared, and the product (PEO-POSS) possessed the obvious resonance signals at 7.18–7.83 ppm and 3.65 ppm, which are assigned to the protons of phenyl groups of POSS and methylene groups of PEO. In addition, there existed two faint resonance signals at 0.85 and 1.62 ppm, which were assigned to the protons of methylene groups closed to Si. ^{1}H NMR results confirmed that PEO-POSS was synthesized successfully.

PEO-POSS was mixed with DGEBA and DDM, and curried at a presetting temperature to afford the epoxy/PEO-POSS nanocomposites. TGA was used to demonstrate the formation of organic-inorganic nanocomposites. Fig. 2 shows the TGA curves of the epoxy/PEO-POSS nanocomposites at air atmosphere from room temperature to 800 °C. Plain epoxy displayed an initial degradation temperatures (T_d's) of 315.2 °C. Incorporation of PEO-POSS increased the values of T_d's, and T_d of epoxy/PEO-POSS nanocomposite containing 50 wt% PEO increased to 364.2 °C. The increased T_d's mainly resulted from the high thermal resistance of POSS cages. Two obvious degradation processes were displayed in the TGA curves. The first mass loss ron appeared at 400–600 °C, which was attributed to the thermo-oxidative degradation of almost organic components. It was found the percentages of decomposition in this range did not follow the initial compositions of the nanocomposites as before. The similar results were also found in some literature [48,49]. It is plausible to propose that the following factors could affect the percentage of degradation in the ron of temperature. First, the real compositions of samples have changed after the initial

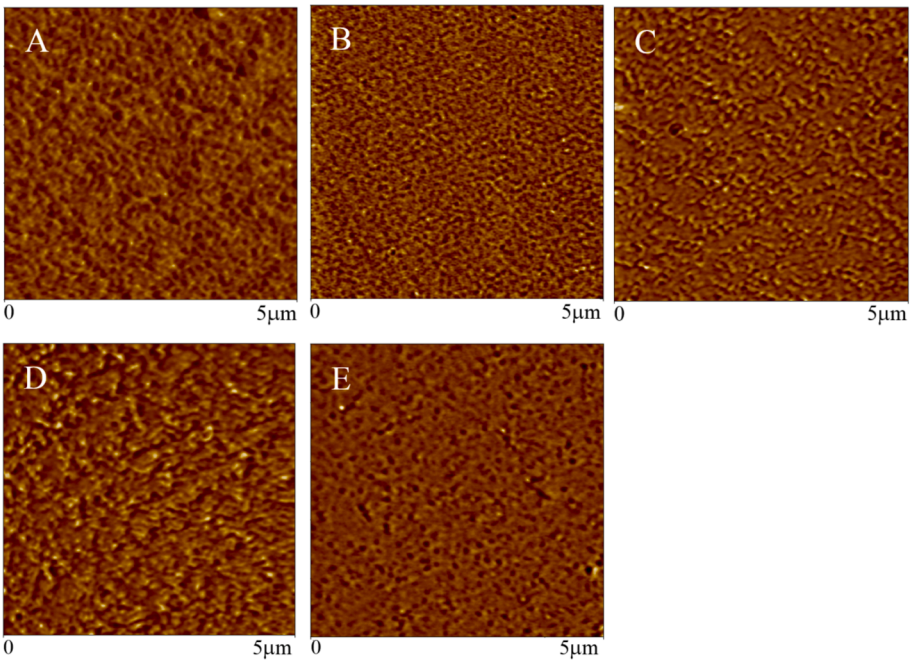

Fig. 7. Surface AFM phase images of epoxy/PEO-POSS nanocomposites containing: 10 A), 20 B), 30 C), 40 D) and E) 50 wt% of PEO.

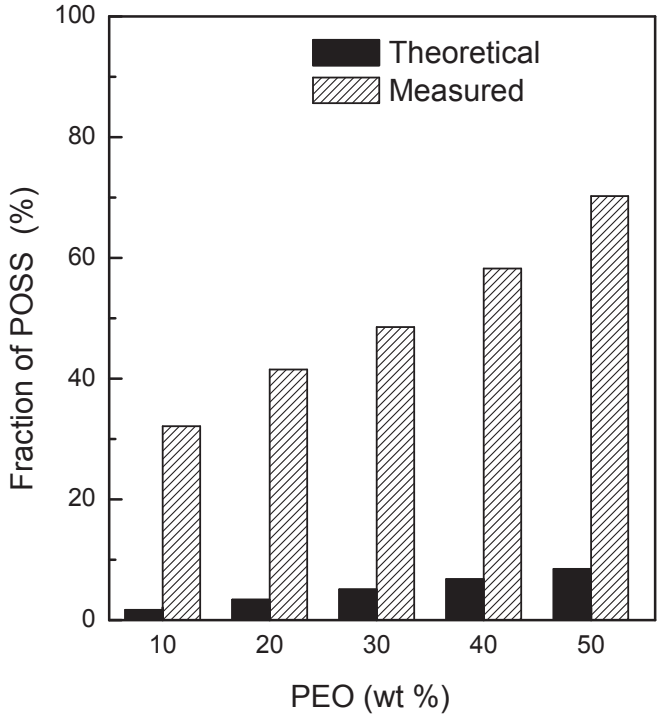

Fig. 8. Fraction of POSS on the surface of epoxy/PEO-POSS nanocomposites.

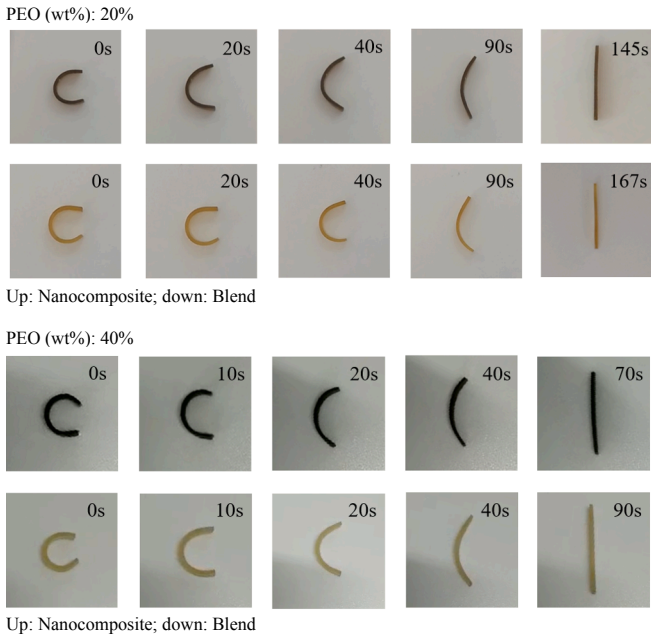

Fig. 9. Shape memory images of epoxy/PEO-POSS nanocomposites and epoxy/PEO blends.

thermal degradation due to the difference in thermal stability among epoxy, PEO and POSS. The percentages of degradation in this ron could only correspond to the real compositions of the degraded samples. Second, the percentages of degradation are quite dependent on the release rates of gaseous substances produced with thermal degradation, which are also quite dependent on the real compositions of the samples after the initial degradation. The second mass loss ron appeared at 600–700 °C, which was attributed to the decomposition of unstable char. It was seen that the thermal stability of epoxy/PEO-POSS nanocomposites was higher than that of the plain epoxy. The increased thermal stability was resulted from two aspects: i) POSS cages displayed high thermal resistance ii) POSS microdomains restricted the release of gaseous products generated during thermal degradation. At above 700 °C, the plain epoxy decomposed completely. In contrast, the epoxy/PEO-POSS nanocomposites showed enhanced residues. The residues were attributed to the char and ceramics from POSS microdomains. According to the values of residues, POSS contents of the nanocomposites can be calculated and the results were summarized in Table 1. It is seen that the POSS contents calculated by TGA was slightly higher than the theoretical values. This phenomenon can be explained that the POSS microdomains restricted the release of gaseous products. As a result, beside the inorganic silica, there remained some chars in the residues.

Since PEO is miscible with epoxy and POSS is immiscible with epoxy, it is expected that PEO-POSS will self-assemble into the microdomains in epoxy matrix before curing, and the curing reaction will fix this nanostructure. The self-assembly behavior was investigated by TEM. Before measurements, the samples were cut into ultra-thin films with the thickness of *c.a.* 100 nm by using a diamond knife. The ultra-thin films were subjected to TEM for the observation of the morphological structure. According to the difference of electric density between POSS and epoxy, the dark spheres corresponded to the POSS microdomains while the light area corresponded to the epoxy/PEO matrix. With the increment of PEO-POSS content, the quality of POSS microdomains increased, meanwhile the size of POSS microdomains also increased from 20 nm to 40 nm. Representatively shown in Fig. 3 was TEM image of epoxy/PEO-POSS nanocomposite with the PEO content of 20 wt%. The dark spheres with the diameter of *c.a.* 20 nm were dispersed in the light matrix. TEM results confirmed the formation of nanostructure in the POSS-containing composites.

3.2. Thermal and mechanical properties

Thermal properties of the epoxy/PEO-POSS nanocomposites were investigated by DMTA. Fig. 4 shows the DMTA curves of the epoxy/PEO-POSS nanocomposites and epoxy/PEO blends. For the epoxy/PEO thermosetting blends, with the increment of PEO content, the glass transition temperature (T_g) of the epoxy thermosets decreased. The decreased T_g was due to the plasticization effect of PEO for the epoxy matrix. When incorporating POSS in the epoxy thermosets, there is a common understanding: POSS does not affect T_g of the epoxy thermosets since POSS is not miscible with epoxy/PEO matrix. However, it was found that T_g of epoxy/PEO-POSS nanocomposites was higher than that of epoxy/PEO blends with the identical PEO content. In addition, with increasing of PEO content, the difference of T_g between epoxy/PEO blends and epoxy/PEO-POSS nanocomposites decreased. For example, T_g of epoxy/PEO-POSS nanocomposite containing 10 wt% PEO was 17 °C higher than that of epoxy/PEO blend containing identical PEO, while the difference of two systems containing 40 wt% PEO decreased to 7 °C. Moreover, the T_g values were almost same when the PEO content was 50 wt%. The values of T_g could be affected by the following aspects. First, some of PEO chains which were near to the POSS microdomains demixed from the matrix. As a consequence, there were lower content of PEO in the epoxy/PEO matrix than the theoretical values. Second, the formation of POSS microdomains led to a nano-reinforcement in the materials. Third, the increment of POSS microdomains increased the free volume of polymer matrix. The first two factors resulted in the increase of T_g, while the last factor resulted in the decrease of T_g. When the POSS content is low, the first two factors dominated the effect on T_g, and thus T_g of epoxy/PEO-POSS nanocomposites were higher than that of epoxy/PEO blends. With increasing of POSS content, the effect of free volume of polymer chains increased, and thus the difference of T_g for both systems decreased. The difference of T_g will affect the properties of the materials. Fig. 4 also reveals the relaxation peak intensity of epoxy/PEO-POSS nanocomposites is slightly lower than that of epoxy/PEO

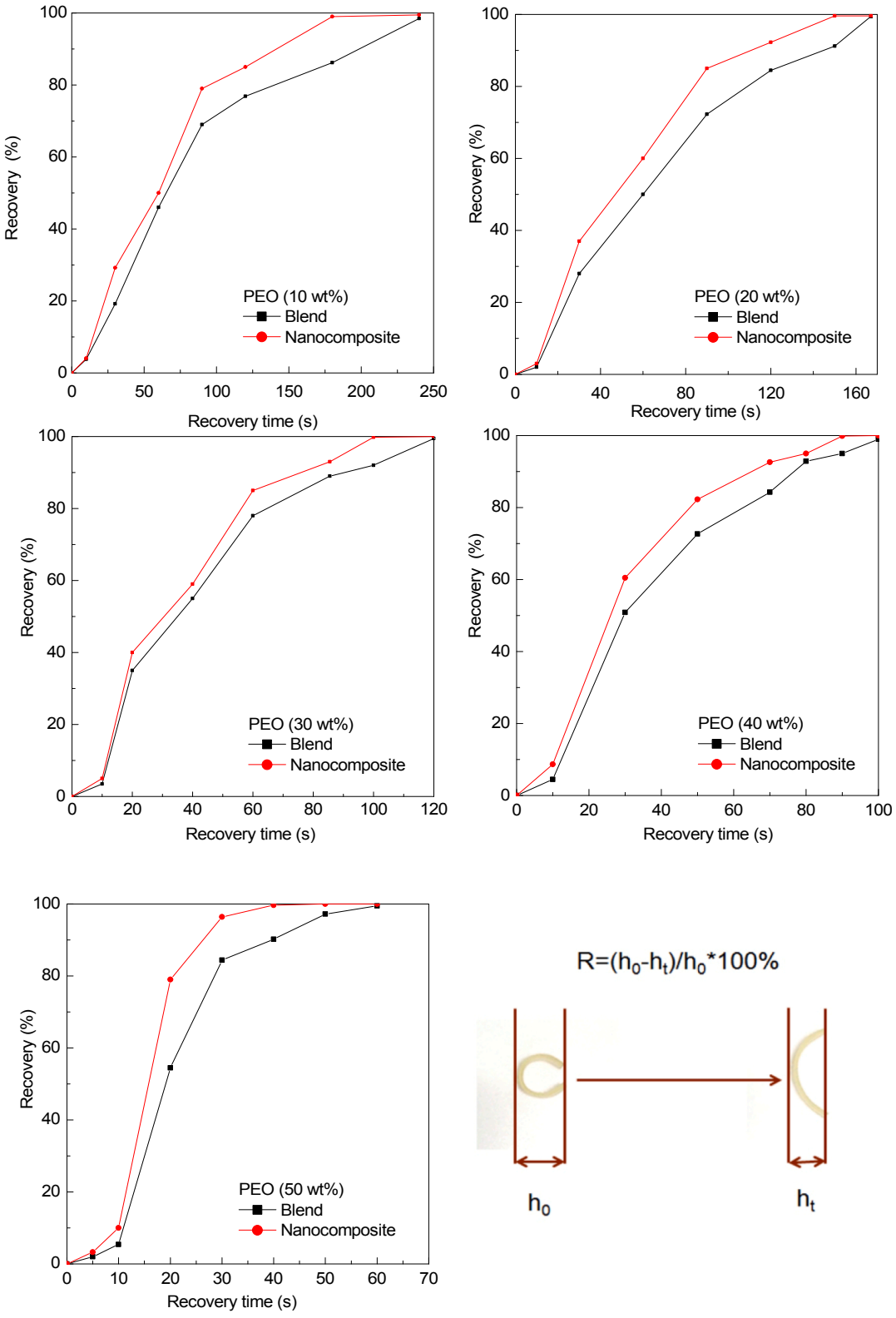

Fig. 10. Recovery of epoxy/PEO blends and epoxy/PEO-POSS nanocomposites.

thermosetting blends with the same PEO content. It declares the existence of POSS physical crosslinking points decreased the molecular mobility of epoxy thermosets, which then resulted in the reduction of relaxation peak intensity.

The mechanical properties of epoxy/PEO-POSS nanocomposites were investigated by tensile measurements. Fig. 5 shows strain-stress curves of epoxy/PEO-POSS nanocomposites and epoxy/PEO blends. The plain epoxy displayed a low strain at break due to the high brittleness. Introduction of PEO and/or PEO-POSS improved the toughness of the materials. The enhanced toughness was reflected by an increasing strain at break (from 1.1% to 14.8%), decreasing maximum stress (from 354 MPa to 10 MPa) with the increment of PEO and/or PEO-POSS

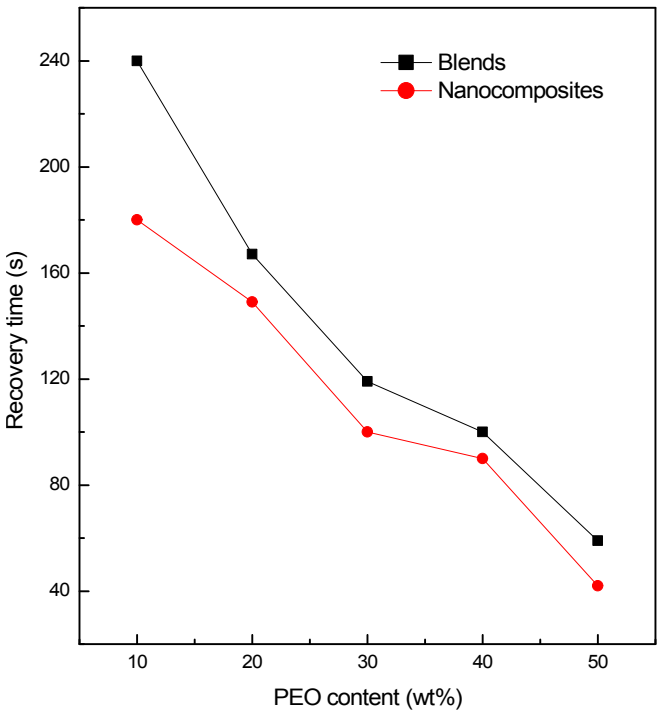

Fig. 11. Recovery time of epoxy/PEO blends and epoxy/PEO-POSS nanocomposites as functions of PEO content.

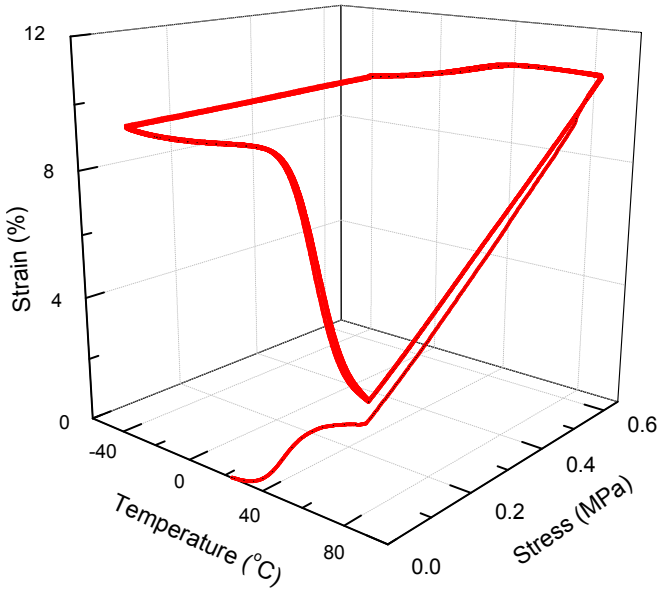

Fig. 12. Shape memory cycle of epoxy/PEO-POSS nanocomposite containing 40 wt% of PEO.

content. Moreover, with the identical content of PEO, the strengths of epoxy/PEO-POSS nanocomposites were higher than that of epoxy/PEO blends. The enhanced tensile strength was attributed to the nano-reinforcement of POSS microdomains in the nanocomposites.

3.3. Surface properties

Due to the inherent low surface energy of organosilicon component, POSS is apt to migrate to the surface of materials, which results in the higher hydrophobicity of the epoxy/PEO-POSS nanocomposites compared with the epoxy/PEO thermosetting blends with the same content of PEO. The surface hydrophobicity can be investigated by the measurement of static contact angle (Fig. 6A). Water and diiodomethane were used as the liquid probes for the measurements. For epoxy/PEO blends, the contact angle decreased with the increment of PEO content due to the hydrophilicity of PEO. When PEO content is 50 wt%, the water contact angle decreased to 10.3°, which was much lower than that of pure epoxy (85.2°). Upon incorporating POSS into epoxy thermosets, the value of contact angle increased. For example, with the same PEO content (50 wt%), the water and diiodomethane contact angle of epoxy/PEO-POSS nanocomposite were 54.8° and 20.3°, which are significantly higher than that of epoxy/PEO blend (10.3° and 9.5°). Based on the values of water and diiodomethane contact angles, the surface free energy of the materials can be calculated [50–52]. The results were summarized in Table 2 and Fig. 6B. With increasing of PEO content, the surface free energy of epoxy/PEO blends increased due to the high free energy and high hydrophilicity of PEO. Compared with epoxy/PEO blends, epoxy/PEO-POSS nanocomposites displayed the lower surface free energy. The reduced surface free energy can be explained that incorporation of POSS changed the distribution of polar groups on the surface of the materials, which affected the hydrophobicity of the materials.

To further investigate the effect of POSS on the surface properties of the epoxy thermosets, we study the distribution of POSS on the surface of the thermosets by observing the surface morphologies. Fig. 7 displayed AFM phase images of the surface of epoxy/PEO-POSS nanocomposites. It is shown the surface of the nanocomposites were microphase separated. The light area is attributed to the POSS microdomains, while the dark area is attributed to the epoxy/PEO matrix. It was displayed that the area of POSS microdomains increased with the content of PEO-POSS. The area fraction of POSS microdomains reveals the distribution of POSS on the surface. We calculated the area fraction of POSS on the surface according to image J software (Fig. 8). Due to the surface enrichment of POSS, the area fractions of POSS on the surface were much higher than the theoretical values. The above results indicated that the formation of POSS microdomains increased the surface hydrophobicity of nanocomposites.

3.4. Shape memory properties

Epoxy polymers are inherently a class of shape memory materials. We introduced PEO-POSS in epoxy resin in order to investigate the influence of POSS microdomains on the shape memory properties of the nanocomposites. The rectangle samples of epoxy/PEO-POSS nanocomposites and epoxy/PEO thermosetting blends were heated at T_1 (*viz.* 20 °C above T_g) for 10 min in oven. They were deformed into a temporary shape ("C" shape) immediately. Afterwards, the samples were quickly dipped in a freezer to fix the shape. For shape recovery measurements, samples with the fixed temporary shape were put on a hot platform at T_1. The photos of different shapes at various stages of the shape memory cycles were recorded. For all epoxy/PEO thermosetting blends and epoxy/PEO-POSS nanocomposites, the recovered shapes were indistinguishable from the original shapes, confirming the excellent shape fixity and recovery. Representatively shown in Fig. 9 are the shape recovery photos of epoxy/PEO-POSS nanocomposites and epoxy/PEO thermosetting blends with PEO content of 20 and 40 wt%, respectively. It was noted that epoxy/PEO thermosetting blends displayed the faster rate of the shape recovery with the increment of PEO content. Epoxy/PEO-POSS nanocomposites displayed faster rate of the shape recovery than that of epoxy/PEO with the same PEO content. We defined the shape recovery rate as the following equation:

$$R = \frac{H_0 - H_t}{H_0}$$

where H_0 is the width of the temporary shape ("C" shape), H_t is the width of recovery shape at t min. Fig. 10 and Fig. 11 displayed the shape

recovery rate as the functions of time and complete shape recovery time as the functions of PEO content, respectively. It was seen both epoxy/PEO blends and epoxy/PEO-POSS nanocomposites displayed excellent shape recovery. With increasing of PEO content, the shape memory time for epoxy/PEO blends and epoxy/PEO-POSS nanocomposites decreased from 240s to 60s and from 180s to 42s, respectively. Moreover, incorporation of POSS enhanced the shape recovery rate. The complete shape recovery time shortened 17–60 s. The accelerated recovery rate can be explained that except for the inherent chemical crosslinking points, additional crosslinking points existed in the epoxy thermosets which resulted from the POSS microdomains.

Shape memory properties were further evaluated using DMTA in a tensile and force controlled mode. Consecutive five shape memory cycles of the epoxy/PEO-POSS nanocomposites and epoxy/PEO blends were recorded. At T_1 (*viz.* 20 °C above T_g), the specimen was elongated at the loading speed of 0.06 MPa/min, allowing the stress up to 0.6 MPa; then the specimen was cooled to T_2 at the rate of 3 °C/min to fix the temporary shapes and then the applied load was removed. Thereafter, the specimen was heated to T_1 at a rate of 3 °C/min to recover the shape. Representatively shown in Fig. 12 are the shape memory cycles of the epoxy/PEO-POSS nanocomposites with PEO content of 40 wt%. There were no noticeable changes of deformation strain, shape fixity and shape recovery occurred after five cycles. The excellent cycling capability is due to the good thermal stability and stable crosslinking structure of the epoxy thermosets, which is in good agreement with the above shape memory measurements.

Shape memory materials possessed the elastomer network, the formation of network resulted from chemical or physical crosslinking of the materials. The external stimulus can change permanent shape into temporary shape. When the materials were applied the external stimulus (heat, photo, electricity *etc.*), the shape will be recovered. Normally, the shape memory properties of common epoxy thermosets resulted from the chemical crosslink network [53,54], and the recovery temperature was above T_g. In this research work, POSS microdomains can be considered as the physical crosslinking points. The shape memory behaviors were a result of the combining chemical and physical crosslinking. In addition, incorporation of PEO-POSS reduced the shape recovery temperature. It provides a facile approach to tailor the thermal transition temperatures of epoxy shape memory polymers.

4. Conclusion

In this work, we synthesized POSS-terminated PEO and investigated the influence of POSS microdomains on the thermal, surface and shape memory properties of homogenous epoxy/PEO thermosetting blends. It was found that the formation of POSS microdomains increased glass transition temperature and storage modulus. POSS immigrated on the surface of the thermosets and thus enhance the surface hydrophobicity of the materials. Epoxy/PEO-POSS nanocomposites displayed accelerated shape recovery rate compared with epoxy/PEO with the same PEO content. The improved shape recovery rate has been addressed on the formation of the physically crosslinked networks in the nanocomposites.

Competing interests

The authors declare no competing interests.

Acknowledgments

The financial supports from National Natural Science Foundation of China (Grant Nos. 21774078, 51133003, 21274091 and 51973113) are acknowledged.

References

[1] Q. Guo, Polymer Blends and Alloys, vol 6, Marcel Dekker, New York, 1999.
[2] S. Zheng, Epoxy Polymers: New Materials and Innovations, vol 5, Wiley-VCH, Weinheim, Germany, 2010, pp. 81–108.
[3] A. Gandini, Epoxy Polymers Based on Renewable Resources, 2010, pp. 55–78.
[4] J. Karger-Kocsis, Epoxy Polymers New Materials and Innovations, Wiley Online Library, Weinheim, Germany, 2010.
[5] A.B. Leonardi, L.A. Fasce, I.A. Zucchi, C.E. Hoppe, E.R. Soulé, C.J. Pérez, R. J. Williams, Eur. Polym. J. 47 (2011) 362–369.
[6] I.A. Rousseau, T. Xie, J. Mater. Chem. 20 (2010) 3431–3441.
[7] S. Park, N. Bernet, S. De La Roche, H. Hahn, J. Compos. Mater. 37 (2003) 465–476.
[8] L. Ruiz-Pérez, G.J. Royston, J.P.A. Fairclough, A.J. Ryan, Polymer 49 (2008) 4475–4488.
[9] C. Zhang, L. Li, S. Zheng, Macromolecules 46 (2013) 2740–2753.
[10] H. Wang, R. Wang, L. Sun, Z. Liu, Y. Zhu, Y. Zhu, RSC Adv. 6 (2016) 45636–45644.
[11] S. Song, K. Park, B. Kim, Y. Choi, G. Jun, D. Lee, B. Kong, K. Paik, S. Jeon, Adv. Mater. 25 (2013) 732–737.
[12] T. Lan, T.J. Pinnavaia, Chem. Mater. 6 (1994) 2216–2219.
[13] J. Zhu, H. Peng, F. Rodriguez-Macias, J.L. Margrave, V.N. Khabashesku, A. M. Imam, K. Lozano, E.V. Barrera, Adv. Funct. Mater. 14 (2004) 643–648.
[14] L.S. Schadler, S.C. Giannaris, P.M. Ajayan, Appl. Phys. Lett. 73 (1998) 3842–3844.
[15] C. Bao, Y. Guo, L. Song, Y. Kan, X. Qian, Y. Hu, J. Mater. Chem. 21 (2011) 13290–13298.
[16] Y. Liu, C. Wu, Y. Chiu, W. Ho, J. Polym. Sci., Part A: Polym. Chem. 41 (2003) 2354–2367.
[17] J. Li, H. Cong, L. Li, S. Zheng, Polymer 69 (2015) 193–203.
[18] J. Li, L. Li, Y. Xiang, S. Zheng, Ind. Eng. Chem. Res. 55 (2016) 586–596.
[19] H. Liu, W. Zhang, S. Zheng, Polymer 46 (2005) 157–165.
[20] L. Li, S. Zheng, Ind. Eng. Chem. Res. 54 (2015) 171–180.
[21] G. Li, L. Wang, H. Ni, C.U. Pittman Jr., J. Inorg. Organomet. Polym. 11 (2001) 123–154.
[22] Y. Abe, T. Gunji, Prog. Polym. Sci. 29 (2004) 149–182.
[23] A. Strachota, I. Kroutilová, J. Kovářová, L. Matějka, Macromolecules 37 (2004) 9457–9464.
[24] L. Matějka, A. Strachota, J. Pleštil, P. Whelan, M. Steinhart, M. Šlouf, Macromolecules 37 (2004) 9449–9456.
[25] W. Chen, Y. Wang, S.W. Kuo, C. Huang, P. Tung, F. Chang, Polymer 45 (2004) 6897–6908.
[26] Z. Zhang, G. Liang, J. Wang, P. Ren, Polym. Compos. 28 (2007) 175–179.
[27] S.W. Kuo, F.C. Chang, Prog. Polym. Sci. 36 (2011) 1649–1696.
[28] F. Alves, I. Nischang, Chem. Eur J. 19 (2013) 17310–17313.
[29] A. Lungu, N.M. Florea, H. Iovu, Polymer 53 (2012) 300–307.
[30] M. Wen, T. Jiang, Y. Ding, Adv. Mater. Res. 1096 (2015) 199–203.
[31] Z. Zhang, A. Gu, G. Liang, P. Ren, J. Xie, X. Wang, Polym. Degrad. Stab. 92 (2007) 1986–1993.
[32] Y. Wang, W. Chen, C. Yang, C. Lin, F. Chang, J. Polym. Sci., Part B: Polym. Phys. 45 (2007) 502–510.
[33] J. Boček, L. Matějka, V. Mentlík, P. Trnka, M. Šlouf, Eur. Polym. J. 47 (2011) 861–872.
[34] A. Lee, J.D. Lichtenhan, Macromolecules 31 (1998) 4970–4974.
[35] M.J. Abad, L. Barral, D.P. Fasce, R.J.J. Williams, Macromolecules 36 (2003) 3128–3135.
[36] J. Choi, J. Harcup, A.F. Yee, Q. Zhu, R.M. Laine, J. Am. Chem. Soc. 123 (2001) 11420–11430.
[37] W. Chen, Y. Wang, S. Kuo, C. Huang, P. Tung, F. Chang, Polymer 45 (2004) 6897–6908.
[38] K. Mishra, G. Pandey, R.P. Singh, Polym. Test. 62 (2017) 210–218.
[39] C. Liu, T. Chen, C. Yuan, Y. Chang, G. Chen, B. Zeng, Y. Xu, W. Luo, L. Dai, RSC Adv. 7 (2017) 46139–46147.
[40] A. Lungu, J. Ghitman, A.I. Cernencu, A. Serafim, N.M. Florea, E. Vasile, H. Iovu, Polymer 145 (2018) 324–333.
[41] L. Wang, S. Zheng, Mater. Chem. Phys. 136 (2012) 744–754.
[42] Y. Ni, S. Zheng, Macromolecules 40 (2007) 7009–7018.
[43] K. Zeng, L. Wang, S. Zheng, X. Qian, Polymer 50 (2009) 685–695.
[44] L. Wang, J. Li, L. Li, S. Zheng, J. Polym. Sci., Part A: Polym. Chem. 51 (2013) 2079–2090.
[45] X. Luo, S. Zheng, N. Zhang, D. Ma, Polymer 35 (1994) 2619–2629.
[46] S. Zheng, N. Zhang, X. Luo, D. Ma, Polymer 36 (1995) 3609–3619.
[47] Y. Cao, S. Xu, L. Li, S. Zheng, J. Polym. Sci., Part B: Polym. Phys. 55 (2017) 587–600.
[48] Y. Xu, Y. Ma, Y. Deng, C. Yang, J. Chen, L. Dai, Mater. Chem. Phys. 125 (2011) 174–183.
[49] Y.C. Chiu, H.C. Tsai, T. Imae, J. Appl. Polym. Sci. 124 (2012) 1234–1240.
[50] D.H. Kaelble, Physical Chemistry of Adhesion, Wiley-Interscience, New York, 1971.
[51] A. Adamson, A.P. Gast, Physical Chemistry of Surfaces, Wiley, New York, 1997.
[52] W.J. Feast, H.S. Munro, R.W. Richards, Polymer Surfaces and Interfaces, Wiley, Chichester, 1993.
[53] T. Xie, I.A. Rousseau, Polymer 50 (2009) 1852–1856.
[54] Y. Liu, C. Han, H. Tan, X. Du, Mater. Sci. Eng. A 527 (2010) 2510–2514.